Crucial role of out-of-plane Sb *p* orbitals in Van Hove singularity formation and electronic correlations in the superconducting kagome metal CsV_3Sb_5

Min Yong Jeong,[1] Hyeok-Jun Yang,[1] Hee Seung Kim,[1] Yong Baek Kim,[2,*] SungBin Lee,[1,†] and Myung Joon Han[1,‡]
[1]*Department of Physics, Korea Advanced Institute of Science and Technology (KAIST), Daejeon 34141, Korea*
[2]*Department of Physics, University of Toronto, Toronto, Ontario M5S 1A7, Canada*

(Received 18 April 2022; revised 13 June 2022; accepted 21 June 2022; published 30 June 2022)

First-principles density functional theory calculations are performed to understand the electronic structure and interaction parameters for recently discovered superconducting kagome metal CsV_3Sb_5. A systematic analysis of the tight-binding parameters based on the maximally localized Wannier function method demonstrates that the out-of-plane Sb^{out}-*p* orbital is a key element in complete description of the three Van Hove singularity structures known in this material at the *M* point near the Fermi level. Further, the correlation strengths are also largely determined by Sb^{out}-*p* states. Based on the constrained random phase approximation, we find that the on-site and intersite interaction parameter are both significantly affected by the screening effect of Sb^{out}-*p* orbitals. As the role of this previously unnoticed orbital state can be tuned or controlled by out-of-plane lattice parameters, we examine the electronic structure and particularly the evolution of Van Hove singularity points as a function of strain and pressure, which can serve as useful knobs to control the material properties.

DOI: 10.1103/PhysRevB.105.235145

I. INTRODUCTION

The recently discovered kagome metal family AV_3Sb_5 ($A = K$, Rb, Cs) has gained a lot of attention by displaying various types of ordered phases intertwined with one another, such as charge density wave (CDW) [1–13] and superconductivity [11–25]. Several different CDW orders have been observed and/or suggested, including the one with broken time-reversal symmetry [2–13,26–33]. Whereas some important experimental features remain controversial [9–11,21–24,34–36], theoretical studies have been actively conducted in order to provide a plausible understanding of their microscopic origins and the interrelationships between different orders, stimulating further explorations [11–13,15–25].

In spite of key insights from previous studies [28–31,37–43], this intriguing material system is still far from being clearly understood. Importantly, the constructed phase diagrams are markedly different from each other, even in the simplest case of single-orbital (typically taking d_{xy} orbital) kagome model calculations at Van Hove filling [39–42]. The resulting superconducting gap symmetry, for example, and the type of charge and spin-density orders are qualitatively different, which is presumably attributed to the parameter choices as well as different numerical techniques. After the discovery of AV_3Sb_5, the two-orbital model (d_{yz} and d_{zx}) has also been adopted [43]. While its results carry invaluable new understanding especially for superconductivity, the difference from or inconsistency with other model studies is still notable. In order to have a better or hopefully complete understanding, it is important to identify the key characterizing factors for the given materials and to obtain realistic material parameters.

In this work we perform a detailed electronic structure calculation of CsV_3Sb_5. We focus on the orbital character of Van Hove singularity (VHS), its dependence on external strain and pressure, and the estimation of interaction strength. By defining the proper local coordinate transformation, we successfully construct the satisfactory orbital characterization of each band and VHS point, which provides a solid ground for model-based theoretical investigations. Remarkably, the out-of-plane Sb^{out}-*p* orbital is found to be crucial in the complete description of the three-VHS feature near the Fermi level (E_F). A systematic MLWF (maximally localized Wannier function) analysis clearly shows that this well-known VHS structure cannot be achieved only with V-*d* orbitals. Further, our cRPA (constrained random phase approximation) calculations reveal that Sb^{out}-*p* also plays a key role in the electronic screening process, thereby determining the effective correlation strengths. The realistic values of both on-site and intersite interaction parameters are presented. By examining the effect of strain and pressure, we explore the possibility to control VHS through Sb^{out}-*p* states.

II. RESULTs AND DISCUSSION

A. Electronic structure and orbital characters

Figure 1(a) shows the crystal structure of CsV_3Sb_5. Separated by the Cs layer, V_3Sb_5 is composed of V_3Sb and two Sb layers. Two distinctive types of Sb, namely, Sb^{in} and Sb^{out}, are located in the same plane with V and above/below the V-Sb^{in} layer, respectively. The V atoms make a kagome network and are surrounded by six Sb atomic octahedron, leading to t_{2g}-e_g crystal field levels. The local structure of the VSb_6

*ybkim@physics.utoronto.ca
†sungbin@kaist.ac.kr
‡mj.han@kaist.ac.kr

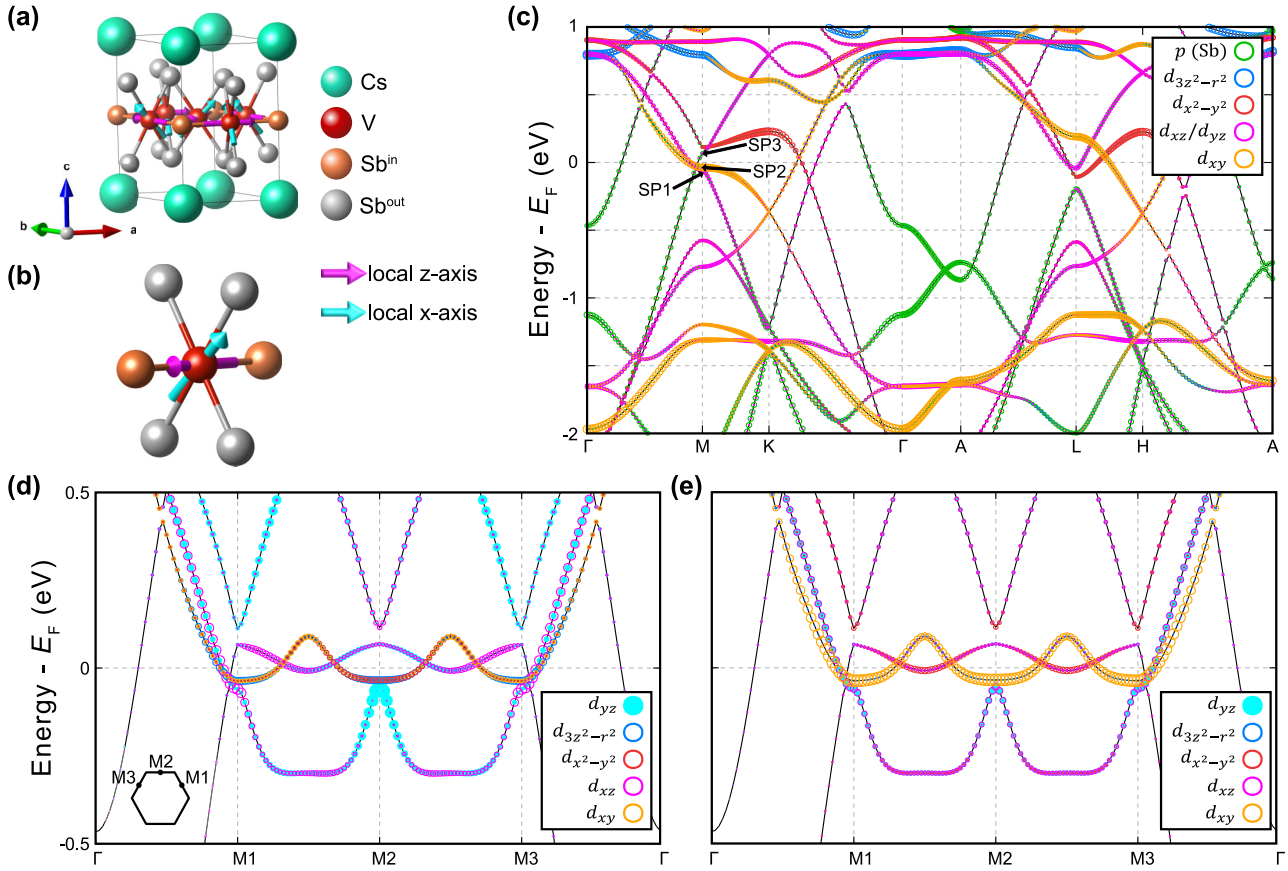

FIG. 1. (a) The crystal structure of CsV_3Sb_5. The cyan, brown, gray, and red spheres represent Cs, Sb^{in}, Sb^{out}, and V atoms, respectively. (b) A local VSb_6 structure, where the x and z axis are depicted by magenta and cyan arrows, respectively. (c) The orbital-projected electronic band structure of CsV_3Sb_5. The orbital projection is performed with the local coordinate as shown in (b). The green, blue, red, magenta, and orange color represent the Sb-p, V-$d_{3z^2-r^2}$, V-$d_{x^2-y^2}$, V-d_{xz}/d_{yz}, and V-d_{xy} characters, respectively, and the circle size shows the relative portion of them. (d), (e) The calculated band dispersion of CsV_3Sb_5 along the line connecting Γ and three symmetric M points. The orbital projection was performed within the (d) global and (e) local axis coordinate.

unit is shown in Fig. 1(b). As discussed further below, it is important to take the proper local coordinate axis in analyzing V-d energy levels, because VSb_6 cages are not aligned along the same direction [see, e.g., Fig. 1(a)]. Since the bond distance from V to Sb^{in} is different from that to Sb^{out}, we take the local z axis along the V–Sb^{in} line [the magenta arrow in Fig. 1(b)], which makes the x and y direction equivalent [the cyan arrow in Fig. 1(b)]. Note that the local z direction is perpendicular to the global c axis of the unit cell; see Fig. 1(a). This choice is also different from that of a previous study [38].

Figure 1(c) shows the orbital-projected band structure. Three saddle points (SPs) are clearly identified near E_F at the M point. These VHSs are the key to understand the intertwining orders in this family of materials. For convenience, we name them SP1, SP2, and SP3 in increasing order of energy. In Figs. 1(d) and 1(e), the energy bands are recast to highlight their orbital characters around three M points. It is noted that only by taking the proper local coordinate axis do the orbital characters of all SPs become symmetric at M.

It is important to note that SP2 is well described by the single-orbital character of d_{xy}. Its portion is ∼70% at all three M points [Fig. 1(e)], which is not the case for the global-axis projection [Fig. 1(d)] in which SP2 has the mixed-orbital character and the composition is different at the three M points. This SP2 VHS is important to understand the competing phases and therefore is taken as the basis for many one-orbital model studies [9,28–31,37,38]. It is also this band dispersion for which the higher-order nature of VHS was highlighted [44,45]. Thus the dominant single-orbital character identified by our local coordinate projection strongly supports this line of one-orbital (or three-band in the unit cell) TB model studies and also the patch models [9,28–31,37–42], providing a solid ground for such theoretical works.

Another notable model approach takes two orbitals of d_{yz}/d_{xz}. For example, it was adopted for a recent RPA study to elucidate the unconventional superconductivity in this system [43]. Also, in the angle-resolved photoemission spectroscopy (ARPES) analysis, the stabilization of CDW and the corresponding spectrum modulation have been discussed based on the two-orbital model [44]. The two-orbital TB Hamiltonian supports two VHSs, corresponding to SP1 and SP3 in our density functional theory (DFT) band, and the higher-lying SP3 is known to play the key role [43,44]. Unraveling the detailed electronic nature of SP3 is therefore of crucial importance.

Figure 1(e) shows that the main V-d character for both SP1 and SP3 is in fact d_{yz}/d_{xz}. As projected onto the proper local coordinate, both orbitals equally participate in the VHSs and the related bands. It can also be seen that SP3 is mixed type

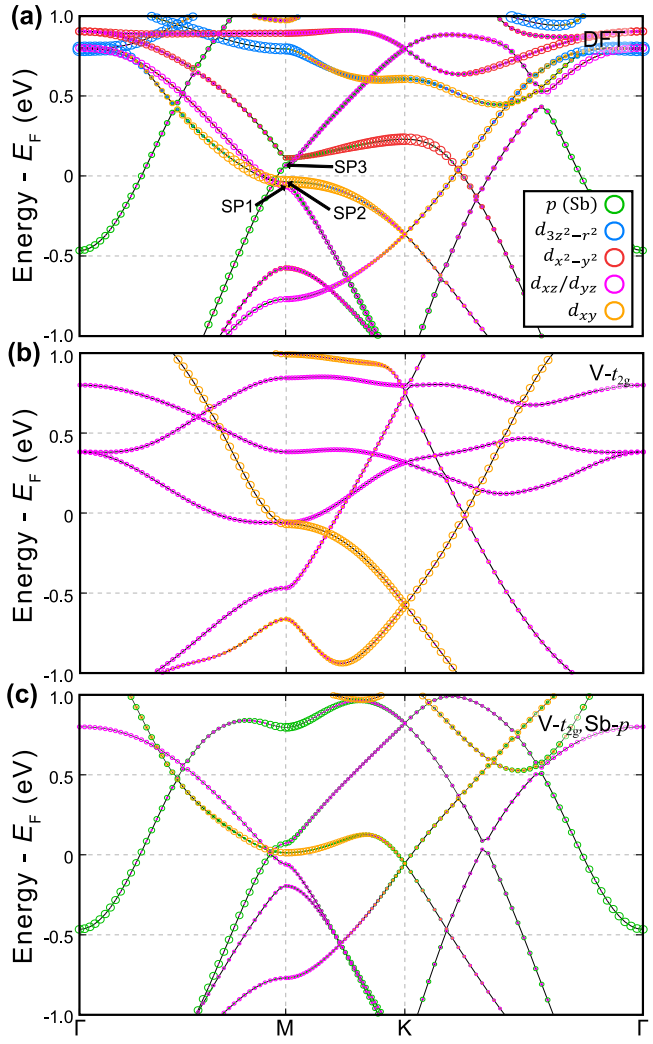

FIG. 2. (a) The electronic band structure computed by DFT. (b, c) The TB band structure as constructed by MLWF method. The TB model contains (b) the V-t_{2g} orbital and (c) V-t_{2g} + Sb-p. The green, blue, red, magenta, and orange circles represent the Sb-p, V-$d_{3z^2-r^2}$, V-$d_{x^2-y^2}$, V-d_{xz}/d_{yz}, and V-d_{xy} character, respectively. The size of circles depicts their portions at given points.

with two-sublattice character, as discussed in the literature [28,43,44]. An important and previously unnoticed feature for SP3 is that V-d is not the major component at SP3. It is in contrast to the cases of SP1 and SP2, which are composed of ∼70% and ∼80% of V-d character, respectively. For SP3, on the other hand, the V-d portion is only ∼32%, and the major contribution comes from Sb^{out}-p, which reaches up to ∼50%, while the Sb^{in}-p contribution is found to be negligible. In the following we further highlight the critical role of the Sb^{out}-p orbital, particularly for the formation of VHS and the screening effect on interaction strength.

B. VHS formation: Tight-binding analysis

To understand the electronic details in the formation of VHSs, we perform a systematic TB analysis. Based on the standard MLWF technique [46,47], we first construct a t_{2g}-only (for each of three V atoms in the unit cell) TB model whose result is presented in Fig. 2(b). Compared with the full-band DFT result shown in Fig. 2(a), it is noted that the main feature of the d_{xy} band and its near-E_F SP nature at the M point are well reproduced, although its dispersion is less flat than the DFT counterpart. Simultaneously, it is obvious that the t_{2g}-only TB Hamiltonian cannot reproduce SP1 and SP3 VHSs: the $d_{xz/yz}$-dominant band shape (magenta colored) is largely different from that in DFT, forming a bare parabolic minimum (rather than a SP) around E_F. Overall, the t_{2g}-only TB model only reproduces SP2 VHS with the noticeably enhanced single-orbital character. With this limitation, it can serve as a good effective model to focus on the VHS point with d_{xy} character [28–31,37–42].

Notably, extending the t_{2g} manifold to the full V-3d orbitals does not make a significant improvement with regard to VHS formation. Our result of the five-orbital TB model is presented in the Appendix B. The main changes by having additional e_g orbitals is the extra bands appearing at higher energy above +0.5 eV, which are in fact mostly of e_g character [see Fig. 5(a) in Appendix B]. Regarding the VHS feature, only slight changes are noticed at the M point in the $d_{xz,yz}$ dispersion and the location of lower-lying VHS (at ~ -0.5 eV). SP1 and SP3 VHSs are still absent in this five-orbital-model result. We note that not only three-orbital t_{2g} but also the five V-d orbital model cannot capture the three VHS features in this material.

Remarkably, the Sb^{out}-p orbitals play the key role in the formation of two more VHSs. Figure 2(c) shows our TB result of the V-t_{2g} + Sb-p model. Not only SP2 (d_{xy}-dominant, yellow colored), but also SP1 (mainly $d_{xz/yz}$ character, magenta colored) and SP3 (mixed $d_{xz/yz}$ character with Sb-p) are clearly identified, although the d_{xy} band becomes deformed near E_F away from the full-band DFT result. In fact, SP3 itself has a sizable portion of Sb-p character. Importantly, it is Sb^{out}-p orbitals that participate in the SP formation, whereas the Sb^{in}-p portion is negligible. As discussed in previous studies [48,49], the main contribution of Sb^{in}-p in the low-energy physics is found in the Γ pocket [see Figs. 2(a) and 2(c)].

Based on our finding, one can understand the formation of low-energy VHS and the intertwining orders in this material. As multiple VHS features are largely affected by Sb^{out}, the energy scale of CDW and other related phases can possibly be changed and controlled by varying the type and/or height of group-V elements. It may also be related to the recently observed three-dimensional structure of the CDW pattern [3–5,7,8,10,12].

C. Interaction strength: cRPA calculations

Electronic interaction is important information for understanding phases in this kagome system. Previous theoretical studies revealed that several different phases can be stabilized by varying interaction parameters. Since the suggested phase diagrams are markedly different from one another depending on both on-site (U) and intersite correlation (V) strengths, as well as the details of model construction and computation [28,39–41,43], it is crucial to estimate realistic values of interaction strengths. One of the most advanced "first-principles" schemes, namely, cRPA, computes the screened Coulomb interactions by systematically removing the partial screenings which are not relevant to a given effective model [50,51]. For

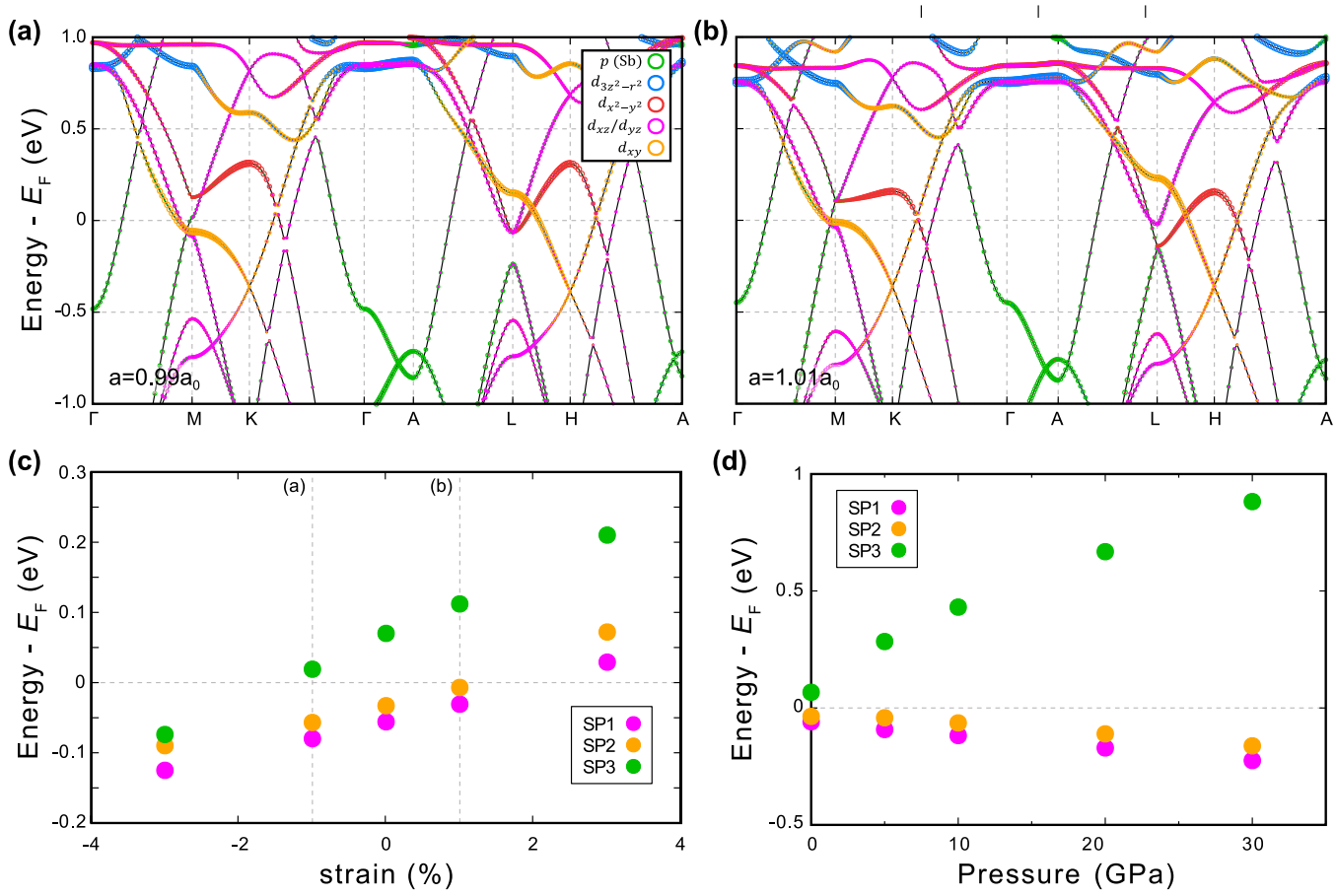

FIG. 3. (a), (b) The orbital-projected electronic band of CsV_3Sb_5 for 1% of (a) compressive and (b) tensile biaxial strain. The green, blue, red, magenta, and orange color represent the Sb-p, V-$d_{3z^2-r^2}$, V-$d_{x^2-y^2}$, V-d_{xz}/d_{yz}, and V-d_{xy} characters, respectively. (c), (d) The calculated energy position of three SPs by varying (c) strain and (d) pressure.

Hubbard-type models with a given correlated subspace, one can therefore calculate the corresponding interaction parameters as wanted. For example, removing the screening effect among V-d and Sb-p yields the value for the "dp model." One can also compute the interaction parameters corresponding to the "d-band-only" Hubbard model by removing only the V-d part (in cRPA literature, called the "d-dp model" [52,53]).

TABLE I. The calculated on-site and intersite interaction parameters for a Hubbard-type model containing correlated V-d orbital states. A systematic cRPA investigation provides the parameters for the given set of removed screenings. It is noted that as more screenings get removed, greater interaction strengths are obtained, as expected. For Hubbard U and Hund J, we follow the definitions as described in Refs. [53–55], for example.

Removed screening	$U(F_0)$ (eV)	J (eV)	V (eV)
All (bare)	15.81	0.78	3.50
V-d, Sb-p	5.33	0.71	1.56
V-d, Sb^{out}-p	2.82	0.68	0.57
V-d, Sb^{in}-p	0.97	0.62	0.10
V-d	0.87	0.61	0.10

Table I presents our cRPA results of on-site interaction parameters Hubbard U and Hund J together with intersite V. As expected, the more screenings removed, the larger the correlation parameters obtained [52,53]. While the "bare" interactions (corresponding to the atomic values) are quite large ($U = 15.81$ and $V = 3.50$ eV), the gradual inclusion of screening effects provides a reasonable estimation of interactions. When the screening effects of both V-d and Sb-p orbitals are removed (i.e., when the dp model is considered), U, J and V are found to be 5.33, 0.71, and 1.56 eV, respectively, in our VASP-cRPA calculation. For more details of computations, see Appendix A. Our dp-model results of $U = 5.3$ and $J = 0.71$ eV are quite close to the values used in a previous dynamical mean-field theory (DMFT) study, supporting their parameter choice [56].

The values from the d-dp model are markedly different. By further excluding Sb-p states, U and V are significantly reduced to 0.87 and 0.10 eV, respectively. While this feature of reduced interactions is a general trend of the d-dp model vs dp model [52], it provides a realistic set of interaction parameters for the widely used d-band-only Hubbard model.

Another remarkable and quite unexpected role of Sb^{out}-p states is found in determining interaction strengths. To examine the role of the Sb^{out}-p state in the screening process, we perform cRPA calculations by separating Sb states into

Sb^{out} and Sb^{in}, and the results are presented in Table I; see the fourth and fifth row. By comparing the result of (V-d, Sb-p) with that of (V-d, Sb^{out}-p) and (V-d, Sb^{in}-p), one can see that the Sb^{out}-p states play a key role in determining correlation strength. The inclusion/exclusion of Sb^{out}-p most significantly affects the parameters. By including only Sb^{out}-p screening (excluding Sb^{in}-p screening) in the dp model, we obtain $U = 0.97$ eV, which is quite close to 0.87 eV of the full d-dp model result (see Appendix A for more details). Hence, most of the screening effects in the d-dp model comes from Sb^{out}-p states, which highlights the important role of Sb^{out} in determining the correlation physics of this material.

Here we recall that the Sb^{out}-p state is important in forming the correct VHS features around E_F as discussed above. It indicates that both VHS physics and the correlation strength can be engineered by controlling Sb^{out}. In iron-based superconductors, the relation of pnictogen height to correlation and magnetic coupling has been highlighted [57–62]. Useful insights may therefore be obtained by examining the change of electronic properties in response to pressure and strain.

D. The effect of biaxial strain and pressure

Both pressure and (uniaxial) strain are proven to be the relevant external stimuli for this material family [15–18,63–65]. Before discussing the change and control of VHSs, let us first check if they are still well defined and the same orbital characters are maintained in an experimentally accessible range of strain. Figures 3(a) and 3(b) show the calculated band structures under 1% of compressive and tensile strain, respectively. The overall dispersion, as well as the orbital characters, are retained, and therefore one can easily identify each of the SPs and monitor their evolution. We find that it is also the case for hydrostatic pressure (not shown). For more information, including the change of the higher-order feature of the SP2 band, see Appendix B.

The evolution of three VHS positions as a function biaxial strain is presented in Fig. 3(c). An obvious trend is clearly observed: Their energy positions all gradually increase as more tensile strain is applied (the in-plane lattice parameter increases). Our result suggests an interesting possibility, that is, the relative position of VHS points can be systematically controlled by strain. At zero strain, for example, SP2 is closest to E_F (corresponding to a zero energy reference in the figure), and it gets even closer at 1% tensile strain. At -1% of (compressive) strain, on the other hand, SP3 is the closest VHS to E_F. Our results imply that the strain-dependent experiment can provide important information about the role of VHSs and/or their cooperations/competitions in this intriguing system.

The effect of pressure is fairly different in this regard. Figure 3(d) shows the calculated SP eigenvalues as a function of hydrostatic pressure. An increasing trend of the SP3 position is clear, which is distinctive from the decreasing SP1 and SP2 positions [48,49]. All three VHS positions move away from E_F, and therefore the order of their relative distances to E_F is unchanged.

SP3 moving toward higher energy by pressure is in contrast to the case of compressive strain in which the reduced in-plane lattice constant makes its position lower in energy. This different behavior can be understood by considering the out-of-plane lattice parameter, which is reduced by applying pressure but enlarged by compressive strain. By calculating the energy-level changes as a function of distance between the Sb^{out} and V_3Sb layer, we found the same trend with the case of strain rather than pressure (not shown). Here we once again notice the role of Sb^{out}-p, which makes a significant contribution to SP3 VHS, while SP1 and SP2 are mainly composed of V-d orbitals. According to recent experiments, SP3 could mainly be responsible for Fermi surface nesting [44]. Also, T_{CDW} decreases as a function of the out-of-plane lattice constant in both strain and pressure experiments [65]. Further study focusing on SP3 might be able to shed new light on many issues in this system.

III. SUMMARY

To summarize, we performed DFT calculations on CsV_3Sb_5 and pointed out the importance of Sb^{out}-p orbitals. Near E_F, three VHSs (V-d_{xy} dominant, V-d_{yz}/d_{xz} dominant, and V-d_{yz}/d_{xz}+Sb-p) were found. By TB model generation, we found that except d_{xy}-dominant VHS, the other two VHSs cannot be formed without the consideration of Sb^{out}-p orbitals. Thus Sb^{out} atoms are responsible for not only the formation of VHSs, but also provide a significant screening effect. Considering the effect of Sb^{out} for the VHS formation and correlation, we proposed to control the VHS features by the strain and pressure, which will change the height of Sb^{out}. For example, the energy level of SP3 is connected to the out-of-plane lattice constant, which can be changed by the strain or pressure. Elucidating the relationship between the energy level of these VHSs and CDW instability would be an outstanding topic for future study.

Note added. When we finalized our writing, a related paper appeared [66] where Di Sante *et al.* investigated the effective Coulomb correlations in kagome metals, including KV_3Sb_5, based on cRPA.

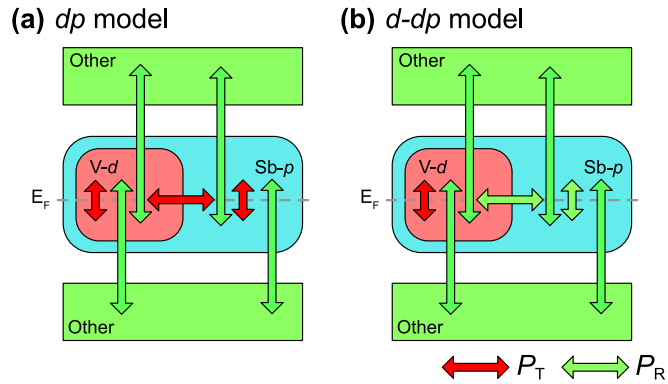

FIG. 4. A schematic picture for (a) cRPA dp model and (b) d-dp model. The red and cyan regions represent the V-d and Sb-p subspace, respectively, as generated by MLWF. The red and green arrows show the polarization corresponding to the target (P_T) and rest space (P_R), respectively.

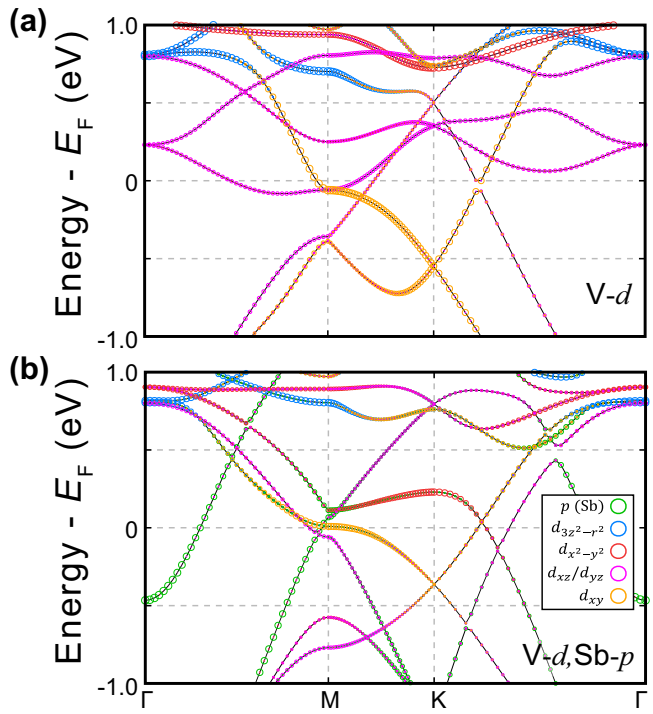

FIG. 5. The TB band structure with (a) V-d ($t_{2g} + e_g$) and (b) V-d plus Sb-p. The green, blue, red, magenta, and orange circles represent the Sb-p, V-$d_{3z^2-r^2}$, V-$d_{x^2-y^2}$, V-d_{xz}/d_{yz}, and V-d_{xy} character, respectively.

ACKNOWLEDGMENTS

M.Y.J. and M.J.H. are supported by a National Research Foundation of Korea (NRF) grant funded by the Korean government (MSIT) (No. 2021R1A2C1009303 and No. 2018M3D1A1058754). M.Y.J. and M.J.H. are supported by the KAIST Grand Challenge 30 Project (KC30) in 2021 funded by the Ministry of Science and ICT of Korea and KAIST (N11210105). H.J.Y., H.S.K., and S.B.L. are supported by NRF Grants No. 2020R1A4A3079707 and No. 2021R1A2C1093060. Y.B.K. is supported by the NSERC of Canada and the Center for Quantum Materials at the University of Toronto.

APPENDIX A: COMPUTATIONAL DETAILS

We carried out first-principles density functional theory (DFT) calculations. For the structural optimizations, we mainly used the Vienna ab initio simulation package (VASP), based on the projector augmented-wave pseudopotential [67,68] within the Perdew-Burke-Ernzerhof (PBE) generalized gradient approximation (GGA) [69]. Both lattice parameters and internal atomic coordinates were optimized with a force criterion of 0.001 eV/Å. The 8×8×4 k points and the 500-eV energy cutoff were adopted. For simulating the strained conditions, the out-of-plane lattice constants and the internal coordinates were calculated at the fixed lateral lattice values. The van der Waals interaction were taken into account within so-called DFT-D3 functional scheme [70]. For the electronic structure analysis, we mainly used the OPENMXsoftware package based on a linear combination of pseudo-atomic-orbital basis [71] and within the PBE-GGA exchange-correlation functional [69]. 12×12×6 k-point grids and a 400-Ry energy cutoff were used. The maximally localized Wannier function (MLWF) method [46,47] was used to construct tight-binding (TB) models. For further orbital-dependent analysis, we also used theDFTFORGE code (which is a part of our JX code) [72].

To calculate the interaction parameters, a constrained random phase approximation (cRPA) calculation was conducted [50,51,73]. For this purpose we used VASP (with WANNIER90 [74]) with a 4×4×2 k mesh. Each orbital space of V-d and Sb-p is defined through the corresponding MLWFs. The on-site interaction parameters U and J are defined following Refs. [53–55]. The nearest-neighboring intersite interaction V is defined as the average value:

$$V = \frac{1}{N} \sum_{i \neq j, \alpha, \beta} W_{i\alpha, i\alpha, j\beta, j\beta}, \tag{A1}$$

where W is the interaction matrix with the sublattice indices i, j, the orbital α, β, and N refers to the number of intersite

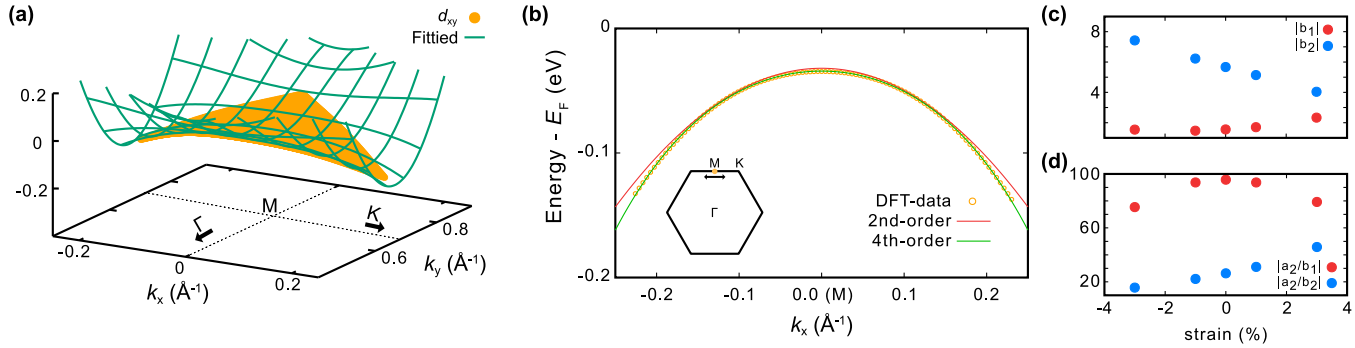

FIG. 6. (a) The calculated eigenvalues (yellow points) near E_F with V-d_{xy} character together with the fitting lines (green) of a fourth-order polynomial. (b) Two different fitting results by the second- (red line) and fourth-order polynomial (green line) in comparison with DFT eigenvalues (orange-colored points). The results are presented along K–M–K line (see inset). In both fittings, all eigenvalues presented in (a) were used. (c) The calculated absolute values of the quadratic terms in the fourth-order polynomial fitting. (d) The absolute value of the ratio between quadratic and quartic constant in the fourth-order fitting.

interaction terms. A part of the results are double-checked with the ECALJ code [75].

As mentioned in the main text, the cRPA procedure provides a systematic estimation of interaction parameters by properly defining the so-called target space and rest space. The effective screened interactions are computed from bare-Coulomb interaction ($\mathcal{V}$) by considering the rest space polarization (P_{R}) as follows [50,51]:

$$U = [1 - \mathcal{V}P_{\mathrm{R}}]^{-1}\mathcal{V}. \tag{A2}$$

To obtain $\mathcal{V}$ and P_{R}, we need to define target space. One conventional approach is using MLWF to define the target and rest spaces [52,53,73,76–79]. Figures 4(a) and 4(b) show the choice of target and rest space corresponding to the so-called dp and d-dp model in cRPA literature. The target space polarization (P_T; red arrows) includes both V-d and Sb-p orbital space in the dp model, and therefore the transitions within V-d, Sb-p, and V-d + Sb-p are taken into account for P_{T}. On the other hand, the so-called d-dp model only takes V-d space as its target space.

APPENDIX B: TIGHT-BINDING ANALYSIS INCLUDING V-e_g ORBITALS

As discussed in the main text, not only the three-band t_{2g} TB Hamiltonian but also the five-V-d band (including both t_{2g} and e_g orbitals) can hardly reproduce the known three-SP structure near E_F. Figure 5(a) shows the result of TB model constructed with all V-d orbitals including e_{g}. Focusing on the near-E_F region, one cannot find significant improvement compared to that of the three-orbital model in Fig. 2(b) with regard, particularly, to Van Hove singularities (VHSs). The main change by the inclusion of e_g orbitals is found at a higher energy range of above 0.5 eV.

The TB result of five V-d and Sb-p is in Fig. 5(b). In comparison with Fig. 2(c) (i.e., V-t_{2g} plus Sb-p), the main change in the close vicinity to E_F is that the downward dispersion of the d_{xy} band (from Γ to M and K) is improved and in better agreement with the DFT result in Fig. 2(a).

APPENDIX C: HIGHER-ORDER NATURE OF SP2 VHS

Novel physical properties driven by higher-order VHS have been an issue in two-dimensional layered materials including kagome systems [80–84]. In fact, recent ARPES studies on CsV_3Sb_5 report the higher-order nature of VHS near E_{F} [44,45]. The control of VHSs by means of pressure, doping, and uniaxial strain has also been discussed in the current system [48,49,65,85,86]. While in the main text we focus on the change of VHSs in response to strain, here we examine the higher-order nature of SP2 and its evolution. We consider the near-M region of $(0.5 \pm 0.1,\ 0.5 \pm 0.1,\ 0)$ and follow the band dispersion with the d_{xy}-orbital portion as a majority. The calculated eigenvalues are plotted in Fig. 6(a) in orange color and then fit to the following equation:

$$E(k_x, k_y) = a_1 k_x^4 + a_2 k_x^2 (k_y - \bar{k}_y)^2 + a_3 (k_y - \bar{k}_y)^4 + b_1 k_x^2 + b_2 (k_y - \bar{k}_y)^2 + c,$$

where k_x (k_y) follows the M-K (Γ-M) line, and $k_x = 0$, $k_y = \bar{k}_y$ for M. The cubic and linear terms are found to be less than 10^{-4}.

TABLE II. The fitting values representing the SP2 VHS dispersion of strained CsV_3Sb_5. The positive and negative strain value refers to the tensile and compressive strain, respectively.

Strain (%)	a_1	a_2	a_3	b_1	b_2	c
−3	0.09	116.59	−61.45	−1.55	7.43	−0.09
−1	−5.55	137.95	−44.61	−1.47	6.23	−0.06
0	−7.77	149.18	−37.13	−1.56	5.67	−0.03
1	−9.39	159.83	−30.71	−1.71	5.14	−0.01
3	−9.78	185.05	−19.23	−2.34	4.04	0.07

The fittinglines are shown in green in Fig. 6(a). The residual sum of squares is 0.0004, and it increases to 0.086 without the quartic term. Figure 6(b) also shows that the inclusion of the fourth-order term gives clearly better agreement with the DFT eigenvalues. It is also consistent with the conclusion from ARPES spectrum analysis [44,45]. Simultaneously, however, the quantitative difference is also noticed. The ARPES fitting found $a_1 = -12.14$ and $b_1 = -1.28$ [44], indicative of the flatter dispersion rather than our DFT result of $a_1 = -7.77$ and $b_1 = -1.56$ (see Table II). It is attributed to the electronic correlation that is not taken into account properly enough within GGA [56]. The higher-order nature of VHS is likely stronger in real material than the DFT result.

The higher-order nature of VHS is also examined as a function of strain. The results are summarized in Table II. As tensile strain is applied, b_1 (corresponding to K–M–K) increases and b_2 (Γ–M–Γ) decreases [see also Fig. 6(c)]. Among the fourth-order terms, a_2 is always the largest and increases as the in-plane lattice parameter increases. To quantify the higher-order nature of SP2 VHS, we computed the ratio between quadratic terms and a_2. Figure 6(d) shows that $|a_2/b_1|$ is maximized at zero strain whereas $|a_2/b_2|$ gradually increases. Interestingly, the higher-order nature is enhanced by tensile strain only along the Γ-M line. In the M–K line it is suppressed.

[1] B. R. Ortiz, L. C. Gomes, J. R. Morey, M. Winiarski, M. Bordelon, J. S. Mangum, I. W. H. Oswald, J. A. Rodriguez-Rivera, J. R. Neilson, S. D. Wilson, E. Ertekin, T. M. McQueen, and E. S. Toberer, Phys. Rev. Materials **3**, 094407 (2019).

[2] N. Shumiya, M. S. Hossain, J.-X. Yin, Y.-X. Jiang, B. R. Ortiz, H. Liu, Y. Shi, Q. Yin, H. Lei, S. S. Zhang, G. Chang, Q. Zhang, T. A. Cochran, D. Multer, M. Litskevich, Z.-J. Cheng, X. P. Yang, Z. Guguchia, S. D. Wilson, and M. Z. Hasan, Phys. Rev. B **104**, 035131 (2021).

[3] B. R. Ortiz, S. M. L. Teicher, L. Kautzsch, P. M. Sarte, N. Ratcliff, J. Harter, J. P. C. Ruff, R. Seshadri, and S. D. Wilson, Phys. Rev. X **11**, 041030 (2021).

[4] H. Li, T. T. Zhang, T. Yilmaz, Y. Y. Pai, C. E. Marvinney, A. Said, Q. W. Yin, C. S. Gong, Z. J. Tu, E. Vescovo, C. S. Nelson, R. G. Moore, S. Murakami, H. C. Lei, H. N. Lee, B. J. Lawrie, and H. Miao, Phys. Rev. X **11**, 031050 (2021).

[5] N. Ratcliff, L. Hallett, B. R. Ortiz, S. D. Wilson, and J. W. Harter, Phys. Rev. Materials **5**, L111801 (2021).

[6] H. Zhao, H. Li, B. R. Ortiz, S. M. L. Teicher, T. Park, M. Ye, Z. Wang, L. Balents, S. D. Wilson, and I. Zeljkovic, Nature (London) **599**, 216 (2021).

[7] M. Kang, S. Fang, J. Yoo, B. R. Ortiz, Y. Oey, S. H. Ryu, J. Kim, C. Jozwiak, A. Bostwick, E. Rotenberg, E. Kaxiras, J. Checkelsky, S. D. Wilson, J.-H. Park, and R. Comin, arXiv:2202.01902.

[8] Y. Hu, X. Wu, B. R. Ortiz, X. Han, N. C. Plumb, S. D. Wilson, A. P. Schnyder, and M. Shi, arXiv:2201.06477.

[9] Y.-X. Jiang, J.-X. Yin, M. M. Denner, N. Shumiya, B. R. Ortiz, G. Xu, Z. Guguchia, J. He, M. S. Hossain, X. Liu, J. Ruff, L. Kautzsch, S. S. Zhang, G. Chang, I. Belopolski, Q. Zhang, T. A. Cochran, D. Multer, M. Litskevich, Z.-J. Cheng *et al.*, Nat. Mater. **20**, 1353 (2021).

[10] D. Song, L. Zheng, F. Yu, J. Li, L. Nie, M. Shan, D. Zhao, S. Li, B. Kang, Z. Wu, Y. Zhou, K. Sun, K. Liu, X. Luo, Z. Wang, J. Ying, X. Wan, T. Wu, and X. Chen, Sci. China Phys. Mech. Astron. **65**, 247462 (2022).

[11] Z. Wang, Y.-X. Jiang, J.-X. Yin, Y. Li, G.-Y. Wang, H.-L. Huang, S. Shao, J. Liu, P. Zhu, N. Shumiya, M. S. Hossain, H. Liu, Y. Shi, J. Duan, X. Li, G. Chang, P. Dai, Z. Ye, G. Xu, Y. Wang *et al.*, Phys. Rev. B **104**, 075148 (2021).

[12] Z. Liang, X. Hou, F. Zhang, W. Ma, P. Wu, Z. Zhang, F. Yu, J.-J. Ying, K. Jiang, L. Shan, Z. Wang, and X.-H. Chen, Phys. Rev. X **11**, 031026 (2021).

[13] H. Chen, H. Yang, B. Hu, Z. Zhao, J. Yuan, Y. Xing, G. Qian, Z. Huang, G. Li, Y. Ye, S. Ma, S. Ni, H. Zhang, Q. Yin, C. Gong, Z. Tu, H. Lei, H. Tan, S. Zhou, C. Shen *et al.*, Nature (London) **599**, 222 (2021).

[14] B. R. Ortiz, S. M. L. Teicher, Y. Hu, J. L. Zuo, P. M. Sarte, E. C. Schueller, A. M. M. Abeykoon, M. J. Krogstad, S. Rosenkranz, R. Osborn, R. Seshadri, L. Balents, J. He, and S. D. Wilson, Phys. Rev. Lett. **125**, 247002 (2020).

[15] K. Y. Chen, N. N. Wang, Q. W. Yin, Y. H. Gu, K. Jiang, Z. J. Tu, C. S. Gong, Y. Uwatoko, J. P. Sun, H. C. Lei, J. P. Hu, and J.-G. Cheng, Phys. Rev. Lett. **126**, 247001 (2021).

[16] F. H. Yu, D. H. Ma, W. Z. Zhuo, S. Q. Liu, X. K. Wen, B. Lei, J. J. Ying, and X. H. Chen, Nat. Commun. **12**, 3645 (2021).

[17] Z. Zhang, Z. Chen, Y. Zhou, Y. Yuan, S. Wang, J. Wang, H. Yang, C. An, L. Zhang, X. Zhu, Y. Zhou, X. Chen, J. Zhou, and Z. Yang, Phys. Rev. B **103**, 224513 (2021).

[18] F. Du, S. Luo, B. R. Ortiz, Y. Chen, W. Duan, D. Zhang, X. Lu, S. D. Wilson, Y. Song, and H. Yuan, Phys. Rev. B **103**, L220504 (2021).

[19] C. Mu, Q. Yin, Z. Tu, C. Gong, H. Lei, Z. Li, and J. Luo, Chin. Phys. Lett. **38**, 077402 (2021).

[20] W. Duan, Z. Nie, S. Luo, F. Yu, B. R. Ortiz, L. Yin, H. Su, F. Du, A. Wang, Y. Chen, X. Lu, J. Ying, S. D. Wilson, X. Chen, Y. Song, and H. Yuan, Sci. China Phys. Mech. Astron. **64**, 107462 (2021).

[21] H.-S. Xu, Y.-J. Yan, R. Yin, W. Xia, S. Fang, Z. Chen, Y. Li, W. Yang, Y. Guo, and D.-L. Feng, Phys. Rev. Lett. **127**, 187004 (2021).

[22] Y. Xiang, Q. Li, Y. Li, W. Xie, H. Yang, Z. Wang, Y. Yao, and H.-H. Wen, Nat. Commun. **12**, 6727 (2021).

[23] Y. Wang, S. Yang, P. K. Sivakumar, B. R. Ortiz, S. M. L. Teicher, H. Wu, A. K. Srivastava, C. Garg, D. Liu, S. S. P. Parkin, E. S. Toberer, T. McQueen, S. D. Wilson, and M. N. Ali, arXiv:2012.05898.

[24] S. Ni, S. Ma, Y. Zhang, J. Yuan, H. Yang, Z. Lu, N. Wang, J. Sun, Z. Zhao, D. Li, S. Liu, H. Zhang, H. Chen, K. Jin, J. Cheng, L. Yu, F. Zhou, X. Dong, J. Hu, H.-J. Gao *et al.*, Chin. Phys. Lett. **38**, 057403 (2021).

[25] C. C. Zhao, L. S. Wang, W. Xia, Q. W. Yin, J. M. Ni, Y. Y. Huang, C. P. Tu, Z. C. Tao, Z. J. Tu, C. S. Gong, H. C. Lei, Y. F. Guo, X. F. Yang, and S. Y. Li, arXiv:2102.08356.

[26] S.-Y. Yang, Y. Wang, B. R. Ortiz, D. Liu, J. Gayles, E. Derunova, R. Gonzalez-Hernandez, L. Šmejkal, Y. Chen, S. S. P. Parkin, S. D. Wilson, E. S. Toberer, T. McQueen, and M. N. Ali, Sci. Adv. **6**, eabb6003 (2020).

[27] F. H. Yu, T. Wu, Z. Y. Wang, B. Lei, W. Z. Zhuo, J. J. Ying, and X. H. Chen, Phys. Rev. B **104**, L041103 (2021).

[28] M. M. Denner, R. Thomale, and T. Neupert, Phys. Rev. Lett. **127**, 217601 (2021).

[29] X. Feng, K. Jiang, Z. Wang, and J. Hu, Sci. Bull. **66**, 1384 (2021).

[30] X. Feng, Y. Zhang, K. Jiang, and J. Hu, Phys. Rev. B **104**, 165136 (2021).

[31] Y.-P. Lin and R. M. Nandkishore, Phys. Rev. B **104**, 045122 (2021).

[32] L. Yu, C. Wang, Y. Zhang, M. Sander, S. Ni, Z. Lu, S. Ma, Z. Wang, Z. Zhao, H. Chen, K. Jiang, Y. Zhang, H. Yang, F. Zhou, X. Dong, S. L. Johnson, M. J. Graf, J. Hu, H.-J. Gao, and Z. Zhao, arXiv:2107.10714.

[33] C. Mielke III, D. Das, J.-X. Yin, H. Liu, R. Gupta, Y.-X. Jiang, M. Medarde, X. Wu, H. C. Lei, J. Chang, P. Dai, Q. Si, H. Miao, R. Thomale, T. Neupert, Y. Shi, R. Khasanov, M. Z. Hasan, H. Luetkens, and Z. Guguchia, Nature (London) **602**, 245 (2022).

[34] T. Neupert, M. M. Denner, J.-X. Yin, R. Thomale, and M. Z. Hasan, Nat. Phys. **18**, 137 (2021).

[35] K. Jiang, T. Wu, J.-X. Yin, Z. Wang, M. Z. Hasan, S. D. Wilson, X. Chen, and J. Hu, arXiv:2109.10809.

[36] H. Tan, Y. Liu, Z. Wang, and B. Yan, Phys. Rev. Lett. **127**, 046401 (2021).

[37] T. Park, M. Ye, and L. Balents, Phys. Rev. B **104**, 035142 (2021).

[38] Y. Gu, Y. Zhang, X. Feng, K. Jiang, and J. Hu, Phys. Rev. B **105**, L100502 (2022).

[39] W.-S. Wang, Z.-Z. Li, Y.-Y. Xiang, and Q.-H. Wang, Phys. Rev. B **87**, 115135 (2013).

[40] M. L. Kiesel, C. Platt, and R. Thomale, Phys. Rev. Lett. **110**, 126405 (2013).

[41] M. L. Kiesel and R. Thomale, Phys. Rev. B **86**, 121105(R) (2012).

[42] S.-L. Yu and J.-X. Li, Phys. Rev. B **85**, 144402 (2012).

[43] X. Wu, T. Schwemmer, T. Müller, A. Consiglio, G. Sangiovanni, D. Di Sante, Y. Iqbal, W. Hanke, A. P. Schnyder, M. M. Denner, M. H. Fischer, T. Neupert, and R. Thomale, Phys. Rev. Lett. **127**, 177001 (2021).

[44] M. Kang, S. Fang, J.-K. Kim, B. R. Ortiz, S. H. Ryu, J. Kim, J. Yoo, G. Sangiovanni, D. Di Sante, B.-G. Park, C. Jozwiak, A. Bostwick, E. Rotenberg, E. Kaxiras, S. D. Wilson, J.-H. Park, and R. Comin, Nat. Phys. **18**, 301 (2022).

[45] Y. Hu, X. Wu, B. R. Ortiz, S. Ju, X. Han, J. Z. Ma, N. C. Plumb, M. Radovic, R. Thomale, S. D. Wilson, A. P. Schnyder, and M. Shi, Nat. Commun. **13**, 2220 (2022).
[46] I. Souza, N. Marzari, and D. Vanderbilt, Phys. Rev. B **65**, 035109 (2001).
[47] N. Marzari and D. Vanderbilt, Phys. Rev. B **56**, 12847 (1997).
[48] A. Tsirlin, P. Fertey, B. R. Ortiz, B. Klis, V. Merkl, M. Dressel, S. Wilson, and E. Uykur, SciPost Phys. **12**, 049 (2022).
[49] H. LaBollita and A. S. Botana, Phys. Rev. B **104**, 205129 (2021).
[50] F. Aryasetiawan, M. Imada, A. Georges, G. Kotliar, S. Biermann, and A. I. Lichtenstein, Phys. Rev. B **70**, 195104 (2004).
[51] F. Aryasetiawan, K. Karlsson, O. Jepsen, and U. Schönberger, Phys. Rev. B **74**, 125106 (2006).
[52] R. Sakuma and F. Aryasetiawan, Phys. Rev. B **87**, 165118 (2013).
[53] L. Vaugier, H. Jiang, and S. Biermann, Phys. Rev. B **86**, 165105 (2012).
[54] V. I. Anisimov, I. V. Solovyev, M. A. Korotin, M. T. Czyżyk, and G. A. Sawatzky, Phys. Rev. B **48**, 16929 (1993).
[55] V. I. Anisimov, F. Aryasetiawan, and A. I. Lichtenstein, J. Phys.: Condens. Matter **9**, 767 (1997).
[56] J. Zhao, W. Wu, Y. Wang, and S. A. Yang, Phys. Rev. B **103**, L241117 (2021).
[57] X. Chen, P. Dai, D. Feng, T. Xiang, and F.-C. Zhang, Natl. Sci. Rev. **1**, 371 (2014).
[58] K. Kuroki, H. Usui, S. Onari, R. Arita, and H. Aoki, Phys. Rev. B **79**, 224511 (2009).
[59] Y. Mizuguchi, Y. Hara, K. Deguchi, S. Tsuda, T. Yamaguchi, K. Takeda, H. Kotegawa, H. Tou, and Y. Takano, Supercond. Sci. Technol. **23**, 054013 (2010).
[60] H. Okabe, N. Takeshita, K. Horigane, T. Muranaka, and J. Akimitsu, Phys. Rev. B **81**, 205119 (2010).
[61] C.-Y. Moon and H. J. Choi, Phys. Rev. Lett. **104**, 057003 (2010).
[62] Z. P. Yin, S. Lebègue, M. J. Han, B. P. Neal, S. Y. Savrasov, and W. E. Pickett, Phys. Rev. Lett. **101**, 047001 (2008).
[63] B. Q. Song, X. M. Kong, W. Xia, Q. W. Yin, C. P. Tu, C. C. Zhao, D. Z. Dai, K. Meng, Z. C. Tao, Z. J. Tu, C. S. Gong, H. C. Lei, Y. F. Guo, X. F. Yang, and S. Y. Li, arXiv:2105.09248.
[64] Y. Song, T. Ying, X. Chen, X. Han, X. Wu, A. P. Schnyder, Y. Huang, J.-G. Guo, and X. Chen, Phys. Rev. Lett. **127**, 237001 (2021).
[65] T. Qian, M. H. Christensen, C. Hu, A. Saha, B. M. Andersen, R. M. Fernandes, T. Birol, and N. Ni, Phys. Rev. B **104**, 144506 (2021).
[66] D. Di Sante, B. Kim, W. Hanke, C. Franchini, R. Thomale, and G. Sangiovanni, arXiv:2203.05038.
[67] G. Kresse and J. Hafner, Phys. Rev. B **48**, 13115 (1993).
[68] G. Kresse and J. Furthmüller, Comput. Mater. Sci. **6**, 15 (1996).
[69] J. P. Perdew, K. Burke, and M. Ernzerhof, Phys. Rev. Lett. **77**, 3865 (1996).
[70] S. Grimme, J. Antony, S. Ehrlich, and H. Krieg, J. Chem. Phys. **132**, 154104 (2010).
[71] T. Ozaki, Phys. Rev. B **67**, 155108 (2003).
[72] H. Yoon, T. J. Kim, J.-H. Sim, and M. J. Han, Comput. Phys. Commun. **247**, 106927 (2020).
[73] E. Şaşıoğlu, C. Friedrich, and S. Blügel, Phys. Rev. B **83**, 121101(R) (2011).
[74] G. Pizzi, V. Vitale, R. Arita, S. Blügel, F. Freimuth, G. Géranton, M. Gibertini, D. Gresch, C. Johnson, T. Koretsune, J. Ibañez-Azpiroz, H. Lee, J.-M. Lihm, D. Marchand, A. Marrazzo, Y. Mokrousov, J. I. Mustafa, Y. Nohara, Y. Nomura, L. Paulatto *et al.*, J. Phys.: Condens. Matter **32**, 165902 (2020).
[75] https://github.com/tkotani/ecalj/.
[76] Y. Nomura, K. Nakamura, and R. Arita, Phys. Rev. B **85**, 155452 (2012).
[77] S. W. Jang, H. Sakakibara, H. Kino, T. Kotani, K. Kuroki, and M. J. Han, Sci. Rep. **6**, 33397 (2016).
[78] T. Miyake and F. Aryasetiawan, Phys. Rev. B **77**, 085122 (2008).
[79] T. Miyake, F. Aryasetiawan, and M. Imada, Phys. Rev. B **80**, 155134 (2009).
[80] A. Ramires, P. Coleman, A. H. Nevidomskyy, and A. M. Tsvelik, Phys. Rev. Lett. **109**, 176404 (2012).
[81] D. V. Efremov, A. Shtyk, A. W. Rost, C. Chamon, A. P. Mackenzie, and J. J. Betouras, Phys. Rev. Lett. **123**, 207202 (2019).
[82] N. F. Q. Yuan, H. Isobe, and L. Fu, Nat. Commun. **10**, 5769 (2019).
[83] H. Isobe and L. Fu, Phys. Rev. Research **1**, 033206 (2019).
[84] L. Classen, A. V. Chubukov, C. Honerkamp, and M. M. Scherer, Phys. Rev. B **102**, 125141 (2020).
[85] A. Consiglio, T. Schwemmer, X. Wu, W. Hanke, T. Neupert, R. Thomale, G. Sangiovanni, and D. Di Sante, arXiv:2111.09342.
[86] Y. M. Oey, B. R. Ortiz, F. Kaboudvand, J. Frassineti, E. Garcia, S. Sanna, V. Mitrović, R. Seshadri, and S. D. Wilson, Phys. Rev. Materials **6**, L041801 (2022)